

A large-scale magnetic shield with 10^6 damping at milli-Hertz frequencies

I. Altarev, M. Bales, K. Fierlinger, P. Fierlinger, F. Kuchler, M. G. Marino, B. Niessen,
G. Petzoldt, J. T. Singh, R. Stoepler, S. Stuibler, M. Sturm, and B. Taubenheim
Physikdepartment, Technische Universität München, D-85748 Garching, Germany

D. H. Beck
University of Illinois at Urbana-Champaign, Urbana, IL 61801, USA

T. Chupp
University of Michigan, Ann Arbor, MI 48109, USA

T. Lins
*Physikdepartment, Technische Universität München, D-85748 Garching, Germany and
FRM-II, Technische Universität München, D-85748 Garching, Germany**

U. Schläpfer
IMEDCO AG, CH-4614 Hägendorf, Switzerland

A. Schnabel and J. Voigt
Physikalisch-Technische Bundesanstalt, 10587 Berlin, Germany
(Dated: March 29, 2022)

A magnetically shielded environment with a damping factor larger than one million at the milli-Hertz frequency regime and an extremely low field and gradient over an extended volume is presented. This extraordinary shielding performance is to our knowledge unprecedented and represents an improvement of the state of the art in damping the difficult regime of very low-frequency distortions by more than an order of magnitude. Thus, a new generation of high precision measurements in fundamental physics and metrology is enabled with this technology, particularly suitable to find traces of new physics far beyond the reach of accelerator based physics. The technical realization of the shield with its improvements in design is discussed.

PACS numbers:

I. INTRODUCTION

Reduction of electromagnetic distortions and temporal variations are crucial parameters for a variety of high precision measurements. High quality magnetic shielding is particularly important for fundamental physics measurements based on spin precession at extremely low magnetic fields. Prominent examples are next generation measurements of electric dipole moments of fundamental particles [1], tests of CPT and Lorentz-invariance and applications of spin clocks [2–4], but also other disciplines, like biomagnetic signal measurements [5] or the investigation of magnetic nanoparticles for cancer therapy [6] use similar techniques.

Precision measurements target the detection of diluted residuals from effects that were dominant in the evolution of the very early universe, far beyond the reach of accelerator-based physics. With many unresolved questions in particle physics in the LHC era, these techniques are getting increased attention. The motivation to develop the shielded environment described here is the new

experiment to measure the time reversal symmetry violating electric dipole moment of the neutron (nEDM) [7]. The nEDM is considered to be one of the most promising systems to actually discover physics beyond the Standard Model. Our planned nEDM experiment is based on two chambers with an overall volume of $\sim 50 \text{ cm} \times 50 \text{ cm} \times 50 \text{ cm}$, filled with spin-polarized species, placed in the center of the shielded environment in an applied magnetic field of 1-2.5 μT . Ramsey's technique [8] is then applied to the spin-polarized species. To ultimately achieve an improvement of the current limit of the nEDM of $2.9 \cdot 10^{-26} \text{ ecm}$ [9] by two orders of magnitude, next to the requirements on the magnitude of the field gradients (for further discussion see e.g. [10]), the temporal stability of the magnetic gradient must be better than 3 pTm^{-1} over 300 s. This requires a strong damping factor of the magnetically shielded environment at extremely low frequencies between 1–100 mHz. Here we describe a magnetic shield with a damping factor for low-amplitude ($\sim 1 \mu\text{T}$) external distortions exceeding 10^6 at the low frequency limit, reducing any distortions caused by any typical external source (crane, people, doors, cars or other machinery in 10's of meters distance from the shield) to below 1 pT. Typical natural ambient

* tobias.lins@ph.tum.de

magnetic field drifts of ~ 100 nT are reduced to ~ 100 fT inside at any point, limiting gradient drifts to ~ 1 pT/m over several hours.

The state-of-the-art for magnetically shielded rooms (MSRs) is the Berlin magnetically shielded room 2 (BMSR-2) [11]. Further, with major improvements in quality and performance of magnetic shields, even smaller residual fields have recently been achieved with much smaller effort, as demonstrated in Ref. [12].

II. THE APPARATUS

Our shield is comprised of a magnetically shielded room (MSR), already described in Ref. [12], forming the outside part of the shield. It consists of two shells made of Magnifer[13], a highly magnetizable alloy. Each shell consists of 2×1 mm thick heat treated Magnifer sheets in a crossed arrangement. A 8 mm thick aluminum shell is placed in between these shells for shielding of higher frequencies. The damping factor for external distortions with frequencies below 0.1 Hz and amplitudes of $2 \mu\text{T}$ peak-to-peak is ~ 280 . Here, the shielding factor SF (damping factor) is defined as

$$SF = \frac{\max(B_0 \sin(\omega t))}{\max(B_{\text{inside}} \sin(\omega t + \phi))}. \quad (1)$$

with ϕ the relative phase of the signal inside the room to the applied signal, B_0 the amplitude of the applied field measured at the position of the center of the shield before the shield is installed, B_{inside} the amplitude of the magnetic field measured in the center of the shield and ω the frequency of the applied AC field. The inside dimensions of the MSR are 2.78 m length, 2.5 m width and 2.35 m height, with 250 mm spacing between the Magnifer shells. The MSR has a door with 1.92 m width and 2 m height, placed symmetrically in a side-wall of the room. Throughout the realization of this shield a set of rules for design principles and construction of magnetic shielding with small residual fields from Ref. [12] has been followed. On the floor, a non-magnetic set of rails with 1.4 m spacing is mounted, which can carry any cuboid load of maximum length 2.78 m \times width 1.92 m \times height 2 m and up to 5.5 tons weight. After the door of the MSR is opened, a detachable set of rails is inserted between the inner rails and an outer table, which continues the rails to a storage area. The detachable section is required to enable closing the door of the MSR. The rails are comprised of plastic wheels with 250 mm spacing along the distance of the rails, an aluminum frame to hold the wheels and titanium bolts as bearings. A manually operated, detachable mechanical winch can be used to slide heavy parts in and out.

On the rails, a cuboid magnetic shield, the 'Insert', with 1.92 m width, 1.92 m height, 2.7 m length and 4 tons weight is placed on the rails. An overview of the assembly with MSR and Insert is shown in Fig. 1. In Fig. 2, a drawing of the insert placed inside and outside

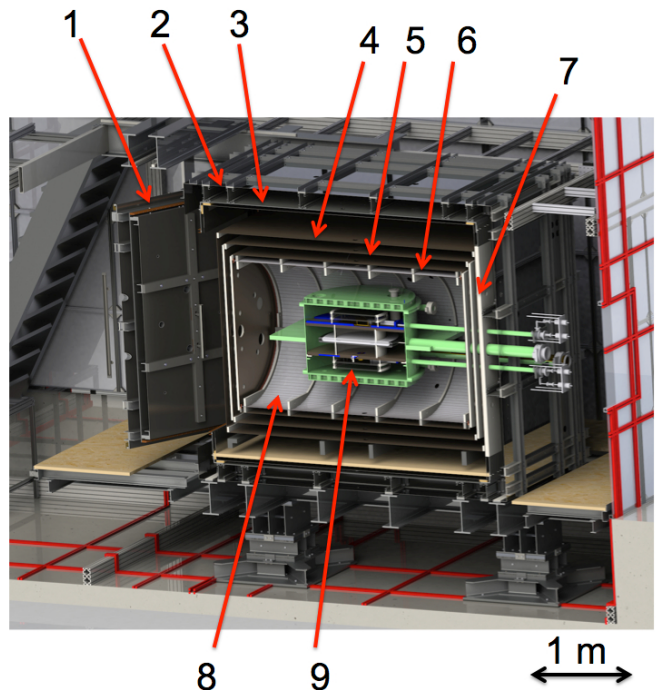


FIG. 1. Cut through the magnetic shield. The outer MSR is described in detail in Ref. [12]. Item (1) is the large door of the MSR, (2) the outer Magnifer shell, (3) the inner Magnifer shell together with the aluminium shell for RF shielding. Inside this shell, a rail system is mounted to bring in the Insert with 3 shells and the experiment. Item (4) is the outer Magnifer shell of the Insert, (5) the middle Magnifer shell and (6) the inner Magnifer shell. The door (7) of the Insert is rigidly mounted to the MSR. Item (8) is a field coil for ultra-low field NMR and (9) the chamber containing an experiment.

of the MSR is shown. The mechanical reproducibility and the alignment of access holes is within 1 mm.

The shield consists of three shells made from Magnifer with 80 mm spacing between the shells. The outer shell has a thickness of 2×1 mm, the middle shell a thickness of 4×1 mm and the innermost shell a thickness of 2×1 mm. The inside dimensions are 1.54 m length \times 1.54 m width \times 2.2 m height, with another rail system inside to optionally slide in another cylindric Magnifer shield (not used here). When slid in, the inner Magnifer shell of the MSR and the outer shell of the Insert are separated by 120 mm in longitudinal (Y) direction, towards the sides the separation is 250 mm and towards top and bottom 220 mm. The door assembly of the Insert is mounted at the inside wall of the MSR, opposite the door, while the whole Insert is removed from the room. This ensures that neither the innermost shell nor any equipment inside is ever exposed to the full strength of the ambient magnetic fields at any time. To close the insert doors, the Insert is slid in manually. A pattern of 16×2.8 m long titanium bolts between the outer and middle shell of the Insert are used to rigidly screw the door inside the MSR to the Insert via a torque-wrench, while the door

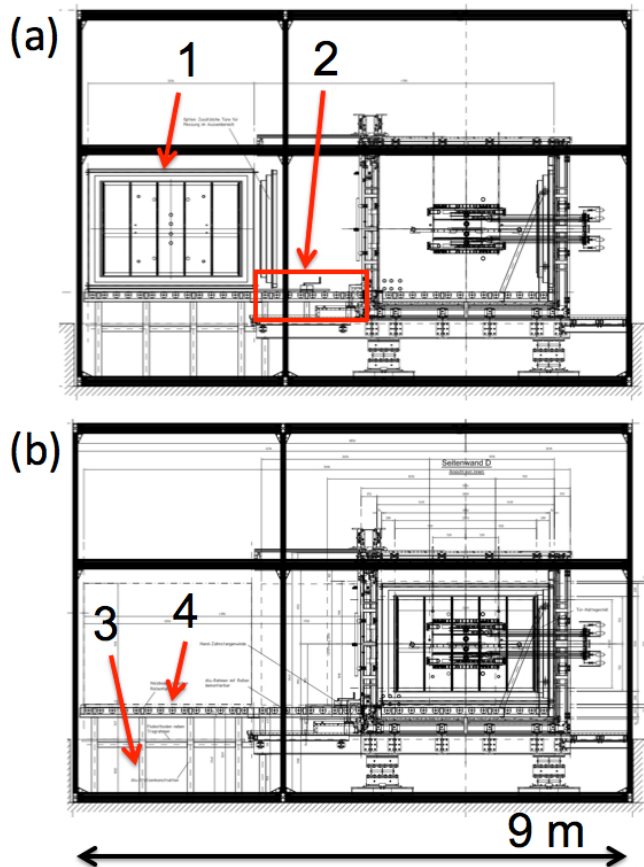


FIG. 2. The Insert placed (a) outside the MSR and (b) inside the MSR. Item (1) is the Insert. It is placed on a table (3) with wheels (4), on which the Insert can be slid into the MSR. A detachable section (2) is required to enable opening and closing of the door.

of the MSR is still open. Both inner doors of the insert are then pressed pneumatically to the inner shells of the Insert. The mechanical force caused by the pneumatic mechanism is carried by the 16 bolts to the main frame of the Insert and is not transferred to the MSR. The gap between the MSR and the Insert on the side and on top is used for sensitive electronics, which can operate without influencing the inner magnetic field, while it still placed inside a low magnetic field with strong RF shielding. No cables for field coils or SQUID signals are exposed to the environment outside the RF shield before amplification. Sensitive electronics can thus stay inside the MSR (and within the RF shield), but outside the Insert.

Magnetic equilibration coils are mounted along the walls of the Insert, but not along the edges of the cuboid shells. Magnetic equilibration is a procedure based on commonly known degaussing techniques [12, 14, 17]. Wiring for magnetic equilibration is done through connectors inside the door of the MSR. Note that no equilibration coils mounted on the doors are necessary. Assembly respectively disassembly of the Insert is done within

10 minutes each, enabling reasonable access to the insert. The door of the MSR is opened by simply pressing one button. Further, 84 penetrations with $> \varnothing 40$ mm and 3 penetrations with $\varnothing 130$ mm enable access for probes and other equipment while the shield is closed. The MSR and the Insert are both portable and independently usable as magnetic shields with similarly good residual field characteristics of 1 m^3 with less than 0.5 nT.

III. MEASUREMENTS

A. Residual field of the insert

A map of the residual field of the Insert after a magnetic equilibration procedure with a not yet fully optimized configuration is shown in Fig. 3, demonstrating that all field values within the inner cubic meter stay well below 1 nT. This is the first test of such an arrangement of equilibration coils not located along the edges. For the determination of the residual field, a Mag03-IEHV70 low-noise fluxgate probe was used. The residual field as function of distance from the surface of the inner magnifer layer is typically below 1 nT at ~ 5 cm distance. For illustration, a measurement of the magnetic field in front of the largest penetrations is shown in Fig. 4. Also at very small distances to the shield walls, the magnetic field is very small.

B. Temporal stability of the insert inside the MSR

A 1000 s long data set of a 10 hours night measurement inside the Insert, which is placed inside the MSR, is shown in Fig. 5. This time interval is about 3-4 times longer than the EDM cycle and within it time corrections for internal field drifts of the liquid-helium cooled SQUID magnetometers have not to be applied. Six SQUID magnetometers are arranged on a cube with a side length of 3 cm, enabling it to measure the magnetic field B_i and the longitudinal gradient $\Delta B_i = \partial B_i / \partial r_i$ in all spatial directions ($B_i = B_x, B_y, B_z$ and $r_i = x, y, z$). The measurement is limited by the noise of the sensor system, only a small real drift in the y - and z -direction is visible. Our results include this noise. For integration times of ~ 300 s all components of the magnetic field are < 100 fT and < 2 pT/m.

C. Shielding performance of individual layers

A notable observation on the side is that the residual field of only the outer layer of the Insert, a 2 mm thick shell of Magnifer, exposed to the earth field and with many penetrations, was below 10 nT measured at the factory site in the same volume after magnetic equilibration, which is a major improvement in performance of single-shell MSRs. The SF at < 0.1 Hz for the outer

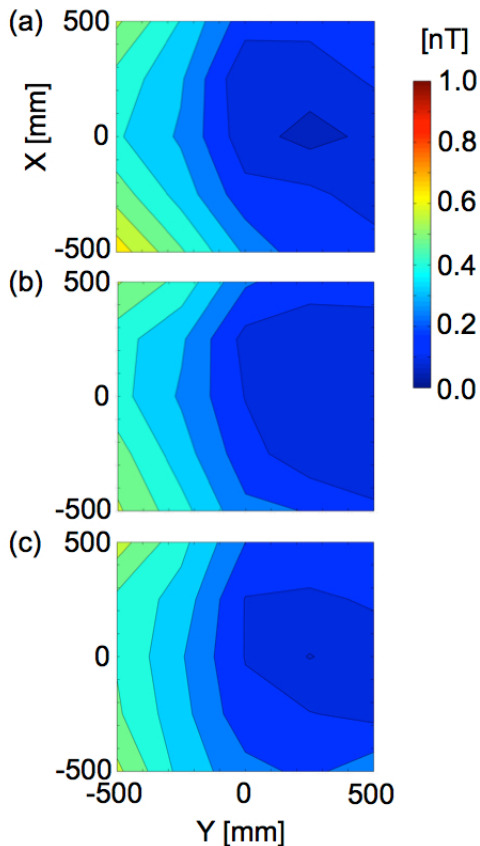


FIG. 3. Absolute value of the magnetic field in the center of the Insert, measured with a fluxgate probe. (a), (b) and (c) are $1 \text{ m} \times 1 \text{ m}$ planes offset in Z direction by -0.25 m , 0 m and $+0.25 \text{ m}$ from the central plane. The measurement pattern is 5×5 points. For this picture, the coordinate center corresponds to the center of the shield. Note that the large distortions are actually not originating from the door with the large holes but from an inserted distortion on the permanently closed side of the Insert.

shell under these conditions is $SF_1 = 40$, for the outer two layers it is $SF_2 = 680$. The thickness of the inner Magnifer shell was deliberately limited to 2 mm to ensure proper magnetic equilibration. It was clearly visible during tests, that the residual field of the 4 mm thick middle layer could not be magnetically equilibrated on the same level due to the availability of the equipment used for this test, resulting in a worse residual field. The measured SFs as function of frequency are shown in Tab. I, together with a comparison of other shields. During this test, the Insert was placed in the earth field and a distortion B_{ext} of $2 \mu\text{T}$ peak-to-peak amplitude at the position of the center of the Insert (measured before placing the Insert on this site) with variable frequency was applied via a 3D quasi-Helmholtz coil system. The sensors used for the different measurements are a fluxgate probe (FG), liquid-helium cooled SQUID magnetometers (SQ), 199-Hg nuclear spin magnetometers (HG) and cesium atomic vapor magnetometers (CS).

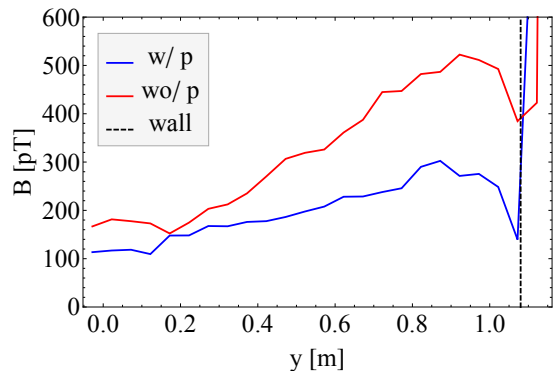


FIG. 4. Magnetic field magnitude measured with a fluxgate along a line concentric in the central 130 mm hole in the back wall of the shield. At distance $y = 0 \text{ m}$ the center of the shield is reached and $y \approx 1.1 \text{ m}$ is the position of the innermost shield layer. The magnetic field was measured with the door closed with (blue) and without (red) pneumatic pressure. In both cases magnetic equilibration was applied. The reproducibility of the measurement is $< 50 \text{ pT}$.

D. Performance of the Insert inside the MSR

The SF has then been measured with the Insert placed inside the MSR. Here, the SF measurements were performed using 199-Hg nuclear- and Cs atomic magnetometers and compared to measurements with a SQUID sensor. As external distortion, four combined coils of the external field compensation system from Ref. [12] were operated as a solenoid in one direction in space. External excitations from $3.2 - 32 \mu\text{T}$ peak-to-peak amplitude at the center of the assembly were applied. The value of the excitation was measured before installation of MSR and Insert at this position. For these measurements, a quartz cell with $\sim 5 \text{ cm}$ diameter, filled with 10^{-5} mbar Hg vapor, is placed in the center of the shield. Two frequency stabilized and carefully tuned 254 nm laser beams penetrate the MSR and the cell horizontally. The transmitted light is detected on the opposite side outside the MSR. A resonant laser beam is used to transversely optically pump the nuclear spins of the 199-Hg isotope along the quantization axis given by the propagation direction of the laser beam. Pumping is done for 3 s with a modulation frequency of the light of $\sim 6.2 \text{ Hz}$, corresponding to the Larmor frequency of 199-Hg in the applied magnetic field $B_0 \sim 0.8 \mu\text{T}$. The polarization is then observed during free precession of the spins for 100 s , an interval chosen to optimally resolve external sinusoidal distortions with 1 mHz amplitude. Typical transverse spin life-times are $> 150 \text{ s}$ for the magnetometer cell, and the sensitivity in 100 s integration time is 12 fT [15]. From this measurement, a distortion inside the MSR+Insert of $13.200 \pm 0.026 \text{ pT}$, caused by $B_{ext} = 16.25 \pm 1 \mu\text{T}$ is observed, equivalent to a $SF(0.001 \text{ Hz}) = (1.23 \pm 0.08) \cdot 10^6$. The systematic effect in the amplitude determination due to the long averaging time for each measured point of 100 s is only few percent and

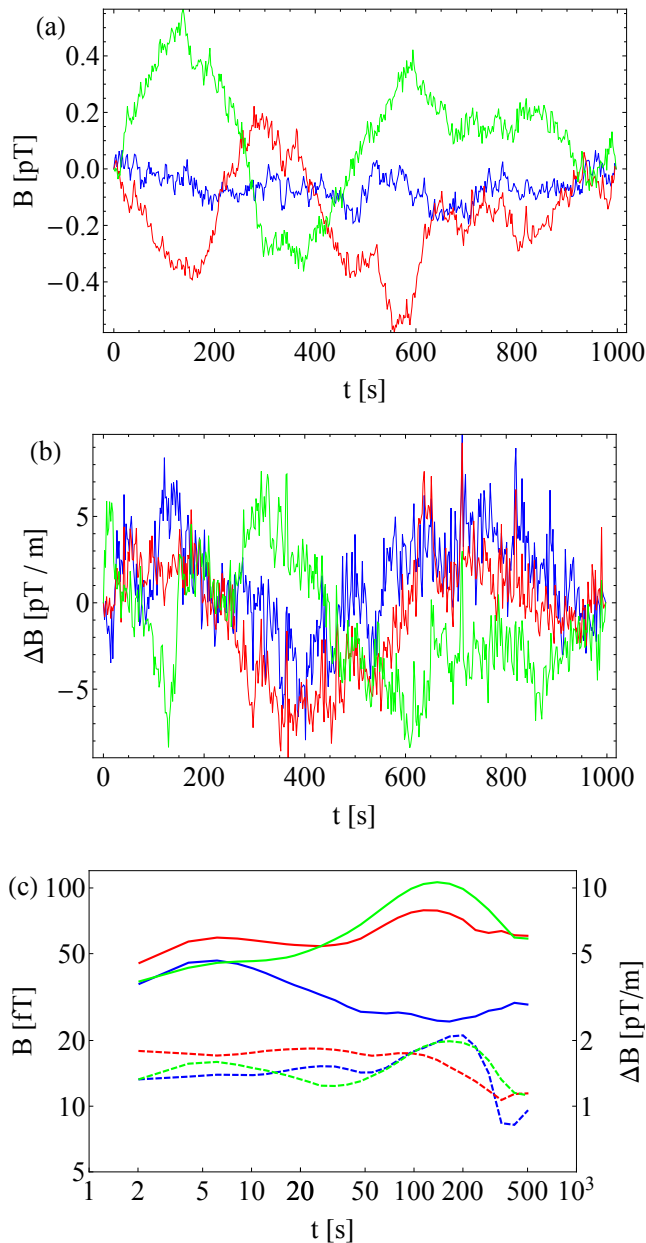


FIG. 5. Temporal stability of the magnetic field in x-, y- and z-direction (blue, red and green) at the center of the the Insert, measured with SQUID magnetometers. (a) is a typical time series of the magnetic field taken during a night under typical conditions. (b) is the gradiometer measurement, simultaneously performed to (a). (c) is the Allan deviation of the magnetic field (solid) and the gradient (dashed) of several 1000 s series.

has been corrected. Due to the time-dependent variation, also the frequency resolution of each measurement is decreased compared to a quasi-static field measurement. The observed deviations between different sensors and the individual measurements are within an acceptable range and expected due to the positioning of the

sensors in the Insert and other geometrical deviations of the outside coils. For comparison, directly on top of the Hg cell a SQUID cryostat is mounted and the signal is measured simultaneously. A simultaneous SQUID measurement in ~ 15 cm to the Hg cell (as close as possible) showed a periodic distortion of 13.850 ± 0.018 pT, or a $SF(0.001 \text{ Hz}) = (1.17 \pm 0.07) \cdot 10^6$, which is compatible with the above numbers. In longitudinal direction of the Insert, the geometric aspect ratio of the inner volume, as well as doors and the placement of all large holes along the path of the magnetic flux reduce the SF notably, as it can be seen in the table for a Hg and a SQUID measurement. Also Cs atomic magnetometers were deployed for comparison and for different measurement conditions. Cs magnetometers [7, 16] use the electronic spin of Cs atoms in an evacuated cell. The spins are optically pumped using alignment pumping and interrogation using linearly polarized laser light, however, with a operation frequency of $\sim 7 \text{ kHz}/\mu\text{T}$. A typical performance of the sensors is pT/\sqrt{Hz} in the configuration used for such measurements. Results of a series of measurements using these sensors are also shown in the table. Due to practical limitations in the simultaneous operation at the same position, all these numbers are within reasonable agreement and show a consistently large SF at very low frequencies. The performance of the HG and CS sensors for SF measurements at even lower frequencies is currently limited by the missing temperature stabilization of the shields, which couple to the applied stable magnetic field and the thermal stability of the laser systems outside the shields. However, these probes are nevertheless better suited than the used SQUID system with a known long-term stability problem to measure long-term drifts.

Note that direct comparison is difficult due to the different measurement conditions used for each MSR. In particular, the geometry of the coils around the MSR and the exact strength of the excitation alter the apparent SF value. In our case, the coils are significantly larger than the MSR ($6 \text{ m} \times 9 \text{ m}$ for transverse/vertical resp. $6 \text{ m} \times 6 \text{ m}$ for longitudinal measurements) and produce a field with a homogeneity of $\sim \pm 20\%$ over the volume of the MSR for the tests. For the case of relatively small Helmholtz-like configurations compared to the dimension of the shield, the SF appears higher due to the intrinsically stronger damping of larger distortions, as they appear locally in this case. For other shields, the coil configuration is unknown or closer to the shield, which alters the SF upwards. It should further be pointed out that shielding becomes significantly more difficult with increased size of the shield. Therefore, the quality of a shield is not only determined by the SF, but rather in comparison of the SF with size and amount of material used for shielding. The SF of the TUM MSR + Insert has been measured using an inhouse fabricated Cs atomic vapor magnetometer and confirmed with a mobile Ltc SQUID system from PTB Berlin. This ensures that the SF measurement is not dominated by systematic issues. The SF measurement is limited by the noise

TABLE I. Measured shielding factors (SF) of different shields as function of external excitation strengths $B_{ext.}$ (peak-to-peak or root mean square) and frequency f for very low frequencies. Estimates for the errors are discussed in the text. For comparison, the SFs of other highly shielded environments are listed.

Shield	f [Hz]	$B_{ext.}$ [μT]	Sensor	SF
MSR outside layers	0.01	2 (pp ^a)	FG	33
MSR both layers (t ^b)	0.01	2 (pp)	FG	279
MSR both layers (l ^c)	0.01	2 (pp)	FG	260
MSR both layers (t)	0.01	32 (pp)	FG	~400
MSR both layers (l)	0.01	32 (pp)	FG	~350
Insert layer 1 (outs.)	0.01	2 (pp)	FG	40
Insert layer 1+2	0.01	2 (pp)	FG	600
Insert (l)	0.01	2 (pp)	FG	4700
Insert (t)	0.01	2 (pp)	FG	6500
Insert (l)	1	2 (pp)	FG	4700
Insert (t)	1	2 (pp)	FG	6500
Insert (l)	10	2 (pp)	FG	56000
Insert (t)	10	2 (pp)	FG	100000
MSR + Insert (l)	0.001	16.25 (pp)	HG	891000
MSR + Insert (l)	0.001	16.25 (pp)	SQ	901500
MSR + Insert (t)	0.001	16.25 (pp)	HG	1231060
MSR + Insert (t)	0.001	16.25 (pp)	SQ	1173300
MSR + Insert (t)	0.001	16.25 (pp)	CS	1390000
MSR + Insert (t)	0.003	16.25 (pp)	CS	1510000
MSR + Insert (t)	0.02	16.25 (pp)	CS	1580000
MSR + Insert (t)	0.05	16.25 (pp)	CS	1660000
MSR + Insert (t)	0.003	3.2 (pp)	SQ	1400000
MSR + Insert (t)	0.01	6.4 (pp)	SQ	2000000
MSR + Insert (t)	0.05	6.4 (pp)	SQ	2130000
MSR + Insert (t)	0.333	32 (pp)	SQ	~8000000
MSR + Insert (t)	1.25	32 (pp)	SQ	> 16700000
BMSR-II	0.01	1 (rms ^d)		75000
BMSR-II	1	1 (rms)		2000000
Boston [18]	0.01	1 (rms)		1630
Boston	1	1 (rms)		200000

^a peak to peak value of a sinusoidal excitation

^b transverse direction

^c longitudinal direction

^d rms value of a sinusoidal excitation

floor and drift of the sensors and applied internal fields. The overall drift of the whole measurement setup, consisting of a Cs magnetometer, the magnetic holding field of $\sim 1 \mu T$ (required for magnetometer operation) and the shield together over night is on the order of 2 pT. The SF measurement has been confirmed with simultaneously performed SQUID magnetometer based measurement, both probes placed approximately in the center of the Insert, with the SQUID on the top.

The magnitude of the magnetic field as function of distance from the walls is comparable to the observations in Ref. [12], basically on the resolution limit of a fluxgate at few centimeter distance from the surface. Another side note is that, the influence of the penetrations does not show a resolvable effect on the residual field in the central cubic meter for three layers or five layers of Magnifer.

IV. CONSIDERATIONS POSSIBLY RELEVANT FOR MAGNETIC SHIELD DESIGN

The configuration uses only a 2 mm thin shell of magnetizable alloy for the innermost shield layer, which allows magnetic equilibration with high quality to obtain very low residual fields. It is clearly possible to sacrifice part of the thickness of the most efficient inner shield layer for the sake of magnetic equilibration without experiencing excessive losses in damping capability. Although the expected performance of our shield is expected to be high compared to the best-shielded room BMSR-2 (cubic design with 3.2 m dimension of the inner Mu-Metal layer [19] due to its smaller size, it was initially unexpected that its performance vastly exceeds the SF of the BMSR-2, with only five layers of Magnifer with (inside to outside) 2-4-2-2-8(aluminum)-2 mm thickness used, compared to seven layers of Mu-Metal in BMSR-2 with thicknesses (inside to outside) 4-7-6-3-10(aluminum)-3-2-2 mm. Major differences in the concept are the thickness of the metal sheets, as well as width and length of individual sheets, which are connected many times to form one closed shell of shielding material. We believe that the better performance is caused by a lower number of joints due to the large sheet size (3000 mm \times 750 mm). We could further demonstrate that the performance of the Insert's SF is high, although the spacing of shield layers is only 80 mm. This contradicts common design criteria, which suggest a significantly larger spacing of the layers to obtain good shielding performance. The arrangement of the magnetic equilibration coils has been chosen in contradiction to previous knowledge: not along the edges of the shield, without notable issues visible in the residual field. The residual field is among the smallest residual fields ever observed over extended volumes and has been demonstrated for the first time for such a large volume fraction. The influence of the holes on the residual field is small already for the 3-layer Insert. With hole diameters of 130 mm, compared to 80 mm layer spacing in the path of the magnetic flux for longitudinally applied external distortions, a surprisingly small distortion in the residual field due to the holes is observed. However, the shielding factor in longitudinal direction actually is lower due to these holes, the doors and the geometrical aspect ratio of the cuboid structure. Three different types of doors with good magnetic shielding properties and low residual field distortions are built in to this shield: a pneumatically clamped door in the outer MSR, a bolted door in the outer layer of the Insert and two pneumatically pressed doors for the two inner layers. Due to the staged tests during construction, the performance of each of the doors could be demonstrated independently. A detailed description of all relevant aspects to achieve ultimate-quality magnetic shielding is in preparation [17].

V. CONCLUSION

The shield described in this manuscript is to our knowledge the by far strongest existing large-scale magnetic shield in terms of magnetic damping factor, although the performance of such installations is difficult to compare directly on this level. In addition, its residual field even with built-in experimental hardware and distortions is extremely small. Many new design concepts have been implemented, including reduced shielding-layer spacing, modified magnetic equilibration coil arrangements, optimized sheet metal arrangements and comparably large penetrations without large distortions on the residual field inside. With a low-frequency SF exceeding 10^6 even for small distortions, our design features potentially has implications on the quality and complexity of shields for next-generation precision experiments.

A cylinder made from Magnifer with 1.4 m diameter, 2 m length and 1.6 mm sheet thickness will further be

added into the insert, acting as a magnet yoke for magnetic holding field of the EDM experiment. This is expected to further increase the SF by a factor of larger than two.

To our knowledge, this installation also represents the currently smallest magnetic field over an extended volume in Milky Way [20] .

ACKNOWLEDGMENTS

We acknowledge the loan of a sensor from PTB Berlin for confirmation of the shielding factors measurement, as well as the support of the machine shops at the FRM-II and at the Physics Department of the TUM in Garching. This work was supported by the DFG Priority Program SPP 1491 and the DFG Cluster of Excellence 'Origin and Structure of the Universe'.

-
- [1] J. Engel, M. J. Ramsey-Musolf, U. van Kolck, Prog. Part. Nuc. Phys. **71** 21 (2013).
 - [2] D. Colladay and V. A. Kostelecky, Phys. Rev. D 55, 6760 (1997).
 - [3] I. Altarev et al., Phys. Rev. Lett. **103**, 081602 (2009).
 - [4] K. Tullney et al., Physical Review Letters, 111, 100801 (2013).
 - [5] L. Trahms, M. Burghoff, Magnetic Resonance Imaging, 28, 1244 (2010).
 - [6] NATO Science for Peace and Security Series B: Physics and Biophysics 99-110 (2014).
 - [7] I. Altarev et al., Il Nuovo Cimento 35 C 122 (2012).
 - [8] N. F. Ramsey, Rev. Mod. Phys. 62, 541 (1990); N. F. Ramsey, Phys. Rev. 76, 996 (1949).
 - [9] C. A. Baker et al., Phys. Rev. Lett. 97, 131801 (2006).
 - [10] J.M. Pendlebury et al., Phys. Rev. **A 70**, 032102 (2004).
 - [11] J. Bork, H. D. Hahlbohm, R. Klein, A. Schnabel, Biomag2000, Proc. 12th Int. Conf. on Biomagnetism, Finland, 970 (2001).
 - [12] I. Altarev et al., Rev. Sci. Instr. 85 , 075106 (2014).
 - [13] Krupp Magnifer 7904.
 - [14] J. Voigt et al., Metrol. Meas. Syst., Vol XX 239 (2013).
 - [15] B. Taubenheim, doctoral thesis, in preparation (2015).
 - [16] S. Pustelny, W. Gawlik, S.M. Rochester, D. F. Jackson Kimball, V.V. Yashchuck, D. Budker, Phys. Rev. A 74, 063420 (2006).
 - [17] St. Stuibler, in preparation (2015).
 - [18] D. Cohen, U. Schlöpfer, S. Ahlfors, M. Hamalainen, E. Halgren, Biomag2002 Proc. (2002).
 - [19] Mu-Metal is a trademark of Vacuumschmelze GmbH, Hanau, Germany.
 - [20] Heliospheric current sheet, http://en.wikipedia.org/wiki/Heliospheric_current_sheet : (2014).